HHS Public Access

Author manuscript

Nano Lett. Author manuscript; available in PMC 2024 June 14.

Published in final edited form as:

Nano Lett. 2023 June 14; 23(11): 5227–5235. doi:10.1021/acs.nanolett.3c01207.

Hydrogel magnetomechanical actuator (h-MMA) nanoparticles for wireless remote control of mechanosignaling *in vivo*

Sumin Jeong[1,2,‡], **Wookjin Shin**[1,‡], **Mansoo Park**[1,3], **Jung-uk Lee**[1], **Yongjun Lim**[1,2], **Kunwoo Noh**[1,3], **Jae-Hyun Lee**[1,3], **Young-wook Jun**[1,3,4,5,6,*], **Minsuk Kwak**[1,3,*], **Jinwoo Cheon**[1,2,3,*]

[1]Center for Nanomedicine, Institute for Basic Science (IBS), Seoul 03722, Republic of Korea

[2]Department of Chemistry, Yonsei University, Seoul 03722, Republic of Korea

[3]Department of Nano Biomedical Engineering (NanoBME), A dvanced Science Institute, Yonsei University, Seoul 03722, Republic of Korea

[4]Department of Otolaryngology, University of California, San Francisco, CA, USA

[5]Department of Pharmaceutical Chemistry, University of California, San Francisco, CA, USA

[6]Helen Diller Family Cancer Comprehensive Center (HDFCCC), University of California, San Francisco, CA, USA

[*]Corresponding Author: Young-wook Jun: Department of Otolaryngology, University of California, San Francisco, San Francisco, California 94158, United States; Department of Pharmaceutical Chemistry, University of California, San Francisco, San Francisco, California 94158, United States; Helen Diller Family Cancer Comprehensive Center (HDFCCC), University of California, San Francisco, San Francisco, California 94158, United States; Center for Nanomedicine, Institute for Basic Science (IBS), Seoul 03722, Republic of Korea; Department of Nano Biomedical Engineering (NanoBME), Advanced Science Institute, Yonsei University, Seoul 03722, Republic of Korea; young-wook.jun@ucsf.edu; Minsuk Kwak: Center for Nanomedicine, Institute for Basic Science (IBS), Seoul 03722, Republic of Korea; Department of Nano Biomedical Engineering (NanoBME), Advanced Science Institute, Yonsei University, Seoul 03722, Republic of Korea; minsuk.kwak@yonsei.ac.kr; Jinwoo Cheon: Center for Nanomedicine, Institute for Basic Science (IBS), Seoul 03722, Republic of Korea; Department of Chemistry, Yonsei University, Seoul 03722, Republic of Korea; Department of Nano Biomedical Engineering (NanoBME), Advanced Science Institute, Yonsei University, Seoul 03722, Republic of Korea; jcheon@yonsei.ac.kr.

[‡]These authors contributed equally to this work.

Authors

Sumin Jeong: Center for Nanomedicine, Institute for Basic Science (IBS), Seoul 03722, Republic of Korea; Department of Chemistry, Yonsei University, Seoul 03722, Republic of Korea; heekyung415@yonsei.ac.kr

Wookjin Shin: Center for Nanomedicine, Institute for Basic Science (IBS), Seoul 03722, Republic of Korea; seramado@yonsei.ac.kr

Mansoo Park: Center for Nanomedicine, Institute for Basic Science (IBS), Seoul 03722, Republic of Korea; Department of Nano Biomedical Engineering (NanoBME), Advanced Science Institute, Yonsei University, Seoul 03722, Republic of Korea; mspark.adm@yonsei.ac.kr

Jung-uk Lee: Center for Nanomedicine, Institute for Basic Science (IBS), Seoul 03722, Republic of Korea; lee7626@yonsei.ac.kr

Yongjun Lim: Center for Nanomedicine, Institute for Basic Science (IBS), Seoul 03722, Republic of Korea; Department of Chemistry, Yonsei University, Seoul 03722, Republic of Korea; yongjun@yonsei.ac.kr

Kunwoo Noh: Center for Nanomedicine, Institute for Basic Science (IBS), Seoul 03722, Republic of Korea; Department of Nano Biomedical Engineering (NanoBME), Advanced Science Institute, Yonsei University, Seoul 03722, Republic of Korea; nkw96@yonsei.ac.kr

ASSOCIATED CONTENT

Supporting Information

Experimental setup for chemical synthesis of hydrogel magnetomechanical actuators (h-MMAs), characterization of h-MMAs, cell line generation and tissue culture, receptor-specific labeling of h-MMAs, *in vitro* experiments including h-MMA labeling, AMF stimulation, immunofluorescence staining, and immunoblotting assay, *in vivo* experiment including xenograft generation, *in vivo* h-MMA delivery and AMF stimulation, immunohistochemistry (IHC), and statistical analyses; Figures S1 – S21; Supplementary Note 1 for the calculation of IPLP values of h-MMA nanoparticles.

Notes

The authors declare no competing financial interests.

Abstract

As a new enabling nanotechnology tool for wireless, target-specific, and long-distance stimulation of mechanoreceptors *in vivo*, here we present a hydrogel magnetomechanical actuator (h-MMA) nanoparticle. To allow both deep-tissue penetration of input signals and efficient force-generation, h-MMA integrates a two-step transduction mechanism that converts magnetic anisotropic energy to thermal energy within its magnetic core (*i.e.*, $Zn_{0.4}Fe_{2.6}O_4$ nanoparticle cluster) and then mechanical energy to induce the surrounding polymer (*i.e.*, pNiPMAm) shell contraction, finally delivering forces to activate targeted mechanoreceptors. We show that h-MMAs enable on-demand modulation of Notch signaling in both fluorescence reporter cell lines and a xenograft mouse model, demonstrating the utility as a powerful *in vivo* perturbation approach for mechanobiology interrogation in a minimally invasive and untethered manner.

Keywords

magnetic nanoparticle cluster; magnetic hyperthermia effect; thermoresponsive hydrogel; mechanosensitive receptor; perturbation biology

Tools for manipulating signaling, activity, and function of specific cells in living organisms have enormous potential to promote novel perturbation biology approaches and unprecedented therapeutic strategies[1–4]. The past decades have witnessed a drastic expansion in physical perturbation methods including nano/micro-electrode arrays[5,6], microfluidics[7,8], optogenetics[9–11], upconversion nanoparticles[12–15], thermogenetic[16–20], sonogenetics[21,22], and mechanogenetics[23,24], enabling neuromodulation, stem cell differentiation, immune cell activation, and cell migration and adhesion with high spatiotemporal precision. However, despite the potential, broad *in vivo* applications of these tools have been lagged by technical limitations. Electrode- or light-based techniques require device implementation into target tissues due to the low tissue penetration depth of input signals[25,26]. Mechanogenetic tools based on force exerted by single magnetic particles under magnetic field gradient only allow short-distance operation, incompatible with animal studies[27,28]. On the other hand, the use of alternating or rotational magnetic field with uniform strength offers long-range stimulation of targeted receptors by converting magnetic anisotropy energy to thermal energy or torque, as demonstrated in magneto-thermogenetic and m-Torquer regulation of specific channel proteins including TRPV and Piezo1, respectively[29–32]. The development of a new tool, that exploits the long-distance operation of the uniform magnetic field while converting the magnetic energy to a different form of physical cue beyond heat or torque, will greatly enhance its useability and applicability to diverse cell signaling processes.

We particularly sought to develop a hydrogel magnetomechanical actuator (h-MMA) nanoparticle that eventually exerts mechanical tensile stress to target proteins in response to oscillatory magnetic field stimulation, as many mechanosensitive proteins relay the signal by unfolding the force-sensing domain upon the application of mechanical pulling[33–38]. Since the direct conversion of magnetic anisotropy energy to mechanical pulling is difficult, we employed a two-step mechanism – magnetic-to-thermal and thermal-to-mechanical transductions, wherein each transduction could be more straightforward by

using magnetic nanoparticles and thermosensitive hydrogel polymers, respectively (Fig. 1a)[39–61]. Specifically, we designed an h-MMA comprised of a magnetic nanoparticle cluster (MNC) core surrounded by a poly N-isopropylmetylacrylamide (pNiPMAm) shell layer. We chose the MNC core to maximize heat generation per particle, while effectively localizing the energy to its surrounding shell layer (detailed discussion in Fig. 2). We also chose pNiPMAm as the shell layer of h-MMA, because of its volume-phase-transition (VPT) behaviors ideally suited for the envisioned application, which include 1) drastic size reduction (up to 75 %) upon VPT, 2) tunable critical transition temperature (T_c) near the body temperature, and 3) facile bio-functionalization. To fabricate h-MMA, we first assembled 13 nm Zn-doped iron oxide ($Zn_{0.4}Fe_{2.6}O_4$) nanoparticles into a superlattice via oil-in-water microemulsion entrapping followed by evaporating the low-boiling point solvent in the oil phase[62–66]. MNCs were coated with a thin SiO_2 (~10 nm) layer and then pNiPMAm via the Stöber method and radical polymerization, respectively (Fig. 1b, See methods for details)[67]. Figure 1c shows representative transmission electron microscope (TEM) images and dynamic light scattering analysis (inset) of MNCs (TEM: 238 ± 28.2 nm, hydrodynamic size: 284 ± 45.1 nm), MNC@SiO_2 (TEM: 260 ± 37.8 nm, hydrodynamic size: 302 ± 83.1 nm), and MNC@SiO_2@pNiPMAm (TEM: 700 ± 50.2 nm, hydrodynamic size: 817 ± 198 nm), confirming the high quality of particles with respect to cluster, size and shape uniformity, and colloidal stability, where these parameters were important for the desired downstream application. To estimate the number density of $Zn_{0.4}Fe_{2.6}O_4$ nanoparticles per MNC, we performed tilted-angle TEM analyses of MNCs along different superlattice crystallographic directions. MNCs have a face-centered-cubic (FCC) cluster with a lattice constant of 20.8 nm suggesting approximately 3,136 particles per MNC (Fig. 1d). The FCC-structured MNCs exhibit maximized nanoparticle packing density (4.44×10^5 particles per μm^3) and therefore higher magnetization (1.249 pemu per MNC @500 Oe), compared to random aggregate counterparts (3.60×10^5 particles per μm^3, 0.982 pemu per random aggregate @500 Oe) (Fig. S1). Accordingly, when assessed magnetic-to-thermal energy conversion capacity via calorimetric bulk solution heating measurement under the application of alternating magnetic fields (AMF at 500 kHz, 500 Oe), a single MNC particle generated approximately 6.83 pW of individual particle power loss (IPLP), 2800 and 1.34 times stronger than a single $Zn_{0.4}Fe_{2.6}O_4$ nanoparticle (2.44 fW) and a random aggregate (5.08 pW), respectively (Fig. 1e, Fig. S2, Supplementary Note 1).

We next tested the capacity of h-MMA (*i.e.,* MNC@SiO_2@pNiPMAm) to transduce heat to mechanical motion by measuring its hydrodynamic size via dynamic light scattering (DLS) while gradually increasing the bulk solution temperature. h-MMA exhibited a clear VPT near 43 °C (*i.e.,* T_c), where the hydrodynamic size gradually decreases from approximately 858 nm to 556 nm with increasing temperature from 30 to 60 °C, respectively, suggesting the collapse of the pNiPMAm layer to 64.8 % of the original size (Fig. 1f)[9,58,60,68]. h-MMA showed stable (variance of the size < 30 nm @ 30 °C with no aggregation), reversible, and sustained VPT behaviors during repeated temperature cycles between 30 °C to 60 °C, confirming the high performance of h-MMAs as thermal-to-mechanical transduction (Fig. 1g, Fig. S3). Previous studies have reported that nanoscale heating of the particle core leads to volume-phase transition of pNiPMAm and the collapse of hydrogel particles on the time scale of ~100 nanoseconds, which allows for h-MMA applications of pN force[58,60].

Together, these two transduction experiments (*i.e.*, AMF-to-bulk heating and bulk heating-to-h-MMA contraction) indicate that h-MMAs are capable of converting an AMF input to the mechanical output signal *via* bulk solution heating using high particle concentration. However, prolonged bulk heating can cause many undesired consequences including cell/tissue damage, nonspecific activation of thermosensitive receptors, and perturbation of extracellular environments. We previously showed that, at a low particle concentration (0.1 mg/ml), magnetic nanoparticle (i.e., 15 nm $CoFe_2O_4$@$MnFe_2O_4$) produced local and transient heating to its vicinity (< 10 nm) (Fig. S4), finally facilitating radical polymerization of vinyl monomers[69]. We hypothesized that the MNC core could induce local heating with more extended ranges, while minimally influencing bulk solution temperature. To test this hypothesis, we synthesized a set of MNC@SiO_2 particles with varied SiO_2 layer thickness (*d*) of approximately 10 (9.7 ± 2.5), 21 (21.4 ± 3.2), 38 (38.3 ± 3.8), and 65 (64.8 ± 5.5) nm, and induced radical polymerization of N-(2-aminoethyl)methacrylate (AEM) under AMF application (500 kHz at 500 Oe, 30 min ON / 30 min OFF cycle for 4 times; Fig. 2a, Fig. S6). We employed a series of thermo-labile azo-molecule radical initiators (initiators A-C) with varied degradation temperatures of 66, 78, and 102 °C at a given experimental condition, respectively (Fig. 2a)[70,71]. We then assessed poly-AEM (*p*AEM) formation on MNC@SiO_2 particles by TEM (Fig. 2b). When *d* equals or below 38 nm and initiators A or B were used, we observed the formation of an additional contrasted layer on MNC@SiO_2, presumably corresponding to *p*AEM. With the initiator C, however, we observed no changes compared with original MNC@SiO_2 particles, suggesting that temperature reached 78 °C but was below 102 °C at $d \leqq 38$ nm. When $d = 65$ nm, we detected the contrasted layer for initiators A but not for B or C, indicating that the temperature at this distance range is approximately 66–78 °C. To test whether the contrasted layer in TEM corresponds to *p*AEM or not, we further reacted as-synthesized particles with amine-reactive fluorescence dyes (Alexa 488-NHS) and counted fluorescence-positive fractions for respective MNC@SiO_2 and initiator combinations under fluorescence microscopy (Fig. 2c, d, Fig. S7). Since the original MNC@SiO_2 particle has no amine functional group but *p*AEM does, positive fluorescence signals after Alexa 488-NHS treatment indicate the *p*AEM layer formation. We observed fluorescence-positive particles only from the samples with the silica thickness and initiator combinations that show additional contrasted layers under TEM, confirming the formation of *p*AEM shells (Fig. 2d, Fig. S7). During AMF stimulation, changes in bulk solution temperature was minimal (Fig. S5). While exact distance-dependent temperature decay profiles from the MNC core remained to be determined, these results confirm that AMF stimulation of MNC can induce significant local heating (> 60 °C) over 60 nm distance ranges from the MNC surface. These results also suggest that AMF stimulation of h-MMA (*i.e.*, MNC@SiO_2@pNiPMAm) can induce VPT (T_c = 43 °C) of a substantial portion of the thermoresponsive layer (*i.e.*, pNiPMAm).

We next examined whether h-MMAs can be used for the envisioned application: target-specific and long-range stimulation of mechanosensitive receptors in cells. As an initial study, we applied h-MMAs to control Notch1 signaling in a cell culture model. We previously showed that Notch1 is a true mechanoreceptor, where mechanogenetic stimulation of Notch1 resulted in its cell surface activation and downstream signaling[24,72,73]. We hypothesized that, when targeted to Notch1, h-MMAs can provide the same

function while allowing long-range stimulation. To allow bio-targeting, fluorescence imaging, and minimal nonspecific binding, we conjugated h-MMAs with single-stranded oligonucleotides, fluorescence dyes (Alexa 488), and polyethylene glycol (PEG), respectively, via click chemistry (see Method sections for details). We then treated a fluorescence reporter U2OS cell line expressing SNAP-Notch1-Gal4 and UAS-H2B-mCherry with benzylguanine-functionalized oligonucleotides bearing complementary sequences (BG-DNA) and oligo-conjugated h-MMAs, sequentially (Fig. 3a). Robust green fluorescence signals were seen at the cell membrane under confocal fluorescence microscopy, suggesting the surface labeling of cells with h-MMA (Fig. S6). Control groups without BG-DNA, using h-MMAs without azide oligonucleotides, or using U2OS cells not expressing SNAP-Notch1 showed negligible fluorescence, confirming target-specific h-MMA labeling (Fig. S8). We then applied AMF (500 kHz at 500 Oe, 30 s ON / 2 min OFF cycle for 15 times, Fig. S9–11, S15) and measured reporter mCherry signals of the cells 24 hr post-stimulation (Fig. 3a). Cells treated with h-MMA and AMF stimulation showed robust nuclear mCherry signals (56.8% mCherry-positive cell fraction; 13.9-fold mean fluorescence intensity) comparable to the cells with Notch receptor-ligand engagement, while those treated with h-MMA (1.38 %; 0.63-fold) or AMF (1.29 %; 0.80-fold) alone showed negligible nuclear fluorescence (Fig. 3b–d, Fig. S12–15) [72,74]. The pNiPMAm particle collapse in response to alternating magnetic field stimulation exerts > 13 pN force per receptor, which is adequate to mechanically activate Notch1[9,24,73]. To directly assess surface activation of Notch, we performed a Western immunoblotting assay that detects cleaved Notch intracellular domain (NICD). Cells treated with both h-MMA and AMF stimulation produced a significantly increased amount of NICD (6.60-fold) compared to the control groups (Fig. 3e). *In vitro* AMF stimulation resulted in minimal bulk solution heating (< 1℃), which has no effect on cell signaling or on cell viability (Fig. S16, 17). These results demonstrate the capacity of h-MMA for specific and targeted stimulation of cells expressing mechanoreceptors.

To demonstrate *in vivo* translation of these successful *in vitro* experiments, we next generated a xenograft mouse model implanted with fluorescence reporter Notch1-U2OS cells described above (Fig. 4a). To establish a bilateral tumor model, 4×10^6 SNAP-Notch1-Gal4 and UAS-H2B-mCherry expressing U2OS cells were subcutaneously implanted into both sides. Mice were provided with the doxycycline (Dox) diet (2 mg/mL) for 8 days to induce robust Notch1 expression in the xenografts (Fig. S18). We injected BG-conjugated h-MMAs intratumorally to the left xenograft site locally, while 30 cycles of AMF stimulation (30 s ON / 2 min OFF for total 75 min) were applied to both sites (Fig. 4a, Fig. S19). After 24 hrs, we sacrificed mice and extracted both tumor masses for immunofluorescence analysis. To detect nuclear mCherry expression, tumors were cryosectioned, immunostained with anti-mCherry antibodies, and imaged under confocal fluorescence microscopy. Consistent with the *in vitro* results, we observed robust mCherry fluorescence signals from the tumor treated with h-MMA and AMF but negligible signals from control groups without Dox, BG-h-MMAs, or applied AMF (Fig. 4b–d), supporting the capacity of h-MMAs for target- and AMF-specific modulation of mechanoreceptors in vivo. To test whether h-MMA causes side effects, we evaluated tissue inflammation and toxicity by immunohistochemical analyses against Iba1. No cytotoxicity or tissue inflammation was

seen due to h-MMAs and/or AMF stimulation *in vivo* (Fig. S20, 21). While promising, biodistribution and systematic clearance of h-MMA have remained to be investigated for its potential clinical uses.

In summary, we developed a novel *in vivo* perturbation platform based on h-MMA nanoparticles. We demonstrated that h-MMA nanoparticles effectively convert magnetic anisotropy energy into mechanical tensile stress to the tethered target molecules via two-step processes involving magnetic-to-thermal and thermal-to-mechanical energy transductions. A similar two-step transduction approach using hydrogel optomechanical actuator nanoparticles for controlling mechanoreceptors *in vitro* has been reported previously[9], but our h-MMA enabled robust deep-tissue stimulation of mechanoreceptors in living organisms using non-invasive and biologically transparent AMF-input. We showed a proof-of-concept study to regulate Notch receptors and downstream synthetic transcription signals, but this generalizable technique can be used to control and understand diverse mechanosensitive receptors in living organisms.

Supplementary Material

Refer to Web version on PubMed Central for supplementary material.

ACKNOWLEDGMENT

This work was supported by Institute for Basic Science (IBS-R026-D1) (M.K. and J.C.), by National Research Foundation of Korea (NRF-2021R1F1A1063378) (M.K.), and by the National Institute of Health and the National Institute of General Medical Science (R35GM134948) (Y.J.).

ABBREVIATIONS

h-MMA	magnetomechanical actuator
m-Torquer	torque-generating magnetic nanoparticle
MNC	magnetic nanoparticle cluster
pNiPMAm	poly N-isopropylmetylacrylamide
VPT	volume-phase-transition
TEM	transmission electron microscope
FCC	face-centered-cubic
AMF	alternating magnetic fields
IPLP	individual particle power loss
DLS	dynamic light scattering
FFT	Fast Fourier Transform
AEM	N-(2-aminoethyl)methacrylate

***p*AEM**	poly-AEM
BG	Benzylguanine
NICD	Notch intracellular domain
PEG	polyethylene glycol
Dox	doxycycline
IHC	immunohistochemistry
ROI	region of interest

REFERENCES

1. Deisseroth K Optogenetics. Nat. Methods 2011, 8, 26. [PubMed: 21191368]
2. Toettcher JE; Voigt CA; Weiner OD; Lim WA The Promise of Optogenetics in Cell Biology: Interrogating Molecular Circuits in Space and Time. Nat. Methods 2011, 8, 35. [PubMed: 21191370]
3. Parnas O; Jovanovic M; Eisenhaure TM; Herbst RH; Dixit A; Ye CJ; Przybylski D; Platt RJ; Tirosh I; Sanjana NE; Shalem O; Satija R; Raychowdhury R; Mertins P; Carr SA; Zhang F; Hacohen N; Regev A A Genome-wide CRISPR Screen in Primary Immune Cells to Dissect Regulatory Networks. Cell 2015, 162 (3), 675. [PubMed: 26189680]
4. Gero M The Optogenetic Catechism. Science 2009, 326 (5951), 395. [PubMed: 19833960]
5. Cogan SF Neural Stimulation and Recording Electrodes. Annu. Rev. Biomed. Eng 2008, 10, 275. [PubMed: 18429704]
6. Guosong H; Lieber CM Novel Electrode Technologies for Neural Recordings. Nat. Rev. Neurosci 2019, 20 (6), 330. [PubMed: 30833706]
7. Sonnen KF; Merten CA Microfluidics as an Emerging Precision Tool in Developmental Biology. Dev. Cell 2019, 48 (3), 293. [PubMed: 30753835]
8. Sonnen KF; Lauschke VM; Uraji J; Falk HJ; Petersen Y; Funk MC; Beaupeux M; François P; Merten CA; Aulehla A Modulation of Phase Shift between Wnt and Notch Signaling Oscillations Controls Mesoderm Segmentation. Cell 2018, 172 (5), 1079. [PubMed: 29474908]
9. Liu Z; Liu Y; Chang Y; Seyf HR; Henry A; Mattheyses AL; Yehl K; Zhang Y; Huang Z; Salaita K Nanoscale Optomechanical Actuators for Controlling Mechanotransduction in Living Cells. Nat. Methods 2016, 13 (2), 143. [PubMed: 26657558]
10. Tischer D; Weiner OD Illuminating Cell Signalling with Optogenetic Tools Nat. Rev. Mol. Cell Biol 2014, 15 (8), 551. [PubMed: 25027655]
11. Zhang K; Cui B Optogenetic Control of Intracellular Signaling Pathways. Trends Biotechnol 2015, 33 (2), 92. [PubMed: 25529484]
12. All AH; Zeng X; Teh DBL; Yi Z; Prasad A; Ishizuka T; Thakor N; Hiromu Y; Liu X Expanding the Toolbox of Upconversion Nanoparticles for in vivo Optogenetics and Neuromodulation. Adv. Mater 2019, 31, 1803474.
13. Chen S; Weitemier AZ; Zeng X; He L; Wang X; Tao Y; Huang AJY; Hashimotodani Y; Kano M; Iwasaki H; Parajuli LK; Okabe S; Teh DBL; All AH; Tsutsui-Kimura I; Tanaka KF; Liu X; McHugh TJ Near-Infrared Deep Brain Stimulation via Upconversion Nanoparticle–Mediated Optogenetics. Science 2018, 359, 679. [PubMed: 29439241]
14. Yi Z; All AH; Liu X Upconversion Nanoparticle-Mediated Optogenetics. Adv. Exp. Med. Biol 2021, 1293, 641. [PubMed: 33398847]
15. Ao Y; Zeng K; Yu B; Miao Y; Hung W; Yu Z; Xue Y; Tan TTY; Xu T; Zhen M; Yang X; Zhang Y; Gao S An Upconversion Nanoparticle Enables Near Infrared-Optogenetic Manipulation of the Caenorhabditis Elegans Motor Circuit. ACS Nano 2019, 13 (3), 3373. [PubMed: 30681836]

16. Chen R; Romero G; Christiansen MG; Mohr A; Anikeeva P Wireless Magnetothermal Deep Brain Stimulation. Science 2015, 347 (6229), 1477. [PubMed: 25765068]
17. Su H; Brockman JM; Duan Y; Sen N; Chhabra H; Bazrafshan A; Blanchard AT; Meyer T; Andrews B; Doye JPK; Ke Y; Dyer RB; Salaita K Massively Parallelized Molecular Force Manipulation with On-Demand Thermal and Optical Control. J. Am. Chem. Soc 2021, 143 (46), 19466. [PubMed: 34762807]
18. Kwizera EA; Stewart S; Mahmud MM; He X Magnetic Nanoparticle-Mediated Heating for Biomedical Applications. J. Heat Transfer 2022, 144 (3), 030801. [PubMed: 35125512]
19. Romero G; Christiansen MG; Barbosa LS; Garcia F; Anikeeva P Localized Excitation of Neural Activity via Rapid Magnetothermal Drug Release. Adv. Funct. Mater 2016, 26, 6471.
20. Rosenfeld D; Senko AW; Moon J; Yick I; Varnavides G; Gregureć D; Koehler F; Chiang PH; Christiansen MG; Maeng LY; Widge AS; Anikeeva P Transgene-Free Remote Magnetothermal Regulation of Adrenal Hormones. Sci. Adv 2020, 6, eaaz3734. [PubMed: 32300655]
21. Maresca D; Lakshmanan A; Abedi M; Bar-Zion A; Farhadi A; Lu GJ; Szablowski JO; Wu D; Yoo S; Shapiro MG Biomolecular Ultrasound and Sonogenetics. Annu. Rev. Chem. Biomol. Eng 2018, 9, 229. [PubMed: 29579400]
22. Fan CH; Wei KC; Chiu NH; Liao EC; Wang HC; Wu RY; Ho YJ; Chan HL; Wang TSA; Huang YZ; Hsieh TH; Lin CH; Lin YC; Yeh CK Sonogenetic-Based Neuromodulation for the Amelioration of Parkinson's Disease. Nano Lett 2021, 21 (14), 5967. [PubMed: 34264082]
23. Zhu L; Wu Y; Yoon CW; Wang Y Mechanogenetics for Cellular Engineering and Cancer Immunotherapy. Curr. Opin. Biotechnol 2020, 66, 88. [PubMed: 32717634]
24. Seo D; Southard KM; Kim JW; Lee HJ; Farlow J; Lee JU; Litt DB; Haas T; Alivisatos AP; Cheon J; Gartner ZJ; Jun YW A Mechanogenetic Toolkit for Interrogating Cell Signaling in Space and Time. Cell 2016, 165, 1507. [PubMed: 27180907]
25. Perlmutter JS; Mink JW Deep Brain Stimulation. Annu. Rev. Neurosci 2006, 29, 229. [PubMed: 16776585]
26. Montgomery KL Yeh AJ; Ho JS; Tsao V; Iyer SM; Grosenick L; Ferenczi EA; Tanabe Y; Deisseroth K; Delp SL; Poon ASY Wirelessly Powered, Fully Internal Optogenetics for Brain, Spinal and Peripheral Circuits in Mice. Nat. Methods 2015, 12 (10), 969. [PubMed: 26280330]
27. Kim JW; Seo D; Lee JU; Southard KM; Lim Y; Kim D; Gartner ZJ; Jun YW; Cheon J Single-Cell Mechanogenetics Using Monovalent Magnetoplasmonic Nanoparticles. Nat. Protoc 2017, 12, 1871. [PubMed: 28817122]
28. Kwak M; Gu W; Jeong H; Lee H; Lee JU; An M; Kim YH; Lee JH; Cheon J; Jun YW Small, Clickable, and Monovalent Magnetofluorescent Nanoparticles (MFNs) Enable Mechanogenetic Regulation of Receptors in a Crowded Live Cell Microenvironment. Nano Lett 2019, 19, 3761. [PubMed: 31037941]
29. Stanley SA; Kelly L; Latcha KN; Schmidt SF; Yu X; Nectow AR; Sauer J; Dyke JP; Dordick JS; Friedman JM Bidirectional Electromagnetic Control of the Hypothalamus Regulates Feeding and Metabolism. Nature 2016, 531 (7596), 647. [PubMed: 27007848]
30. Munshi R; Qadri SM; Zhang Q; Rubio IC; Pino P; Pralle A Magnetothermal Genetic Deep Brain Stimulation of Motor Behaviors in Awake, Freely Moving Mice. Elife 2017, 6, e27069. [PubMed: 28826470]
31. Lee JU; Shin W; Lim Y; Kim J; Kim WR; Kim H; Lee JH; Cheon J Non-Contact Long-Range Magnetic Stimulation of Mechanosensitive Ion Channels in Freely Moving Animals. Nat. Mater 2021, 20, 1029. [PubMed: 33510447]
32. Shin W; Jeong S; Lee JU; Jeong SY; Shin J; Kim HH; Cheon J; Lee JH Magnetogenetics with Piezo1 Mechanosensitive Ion Channel for CRISPR Gene Editing. Nano Lett 2022, 22 (18), 7415. [PubMed: 36069378]
33. Wang X; Ha TJ Defining Single Molecular Forces Required to Activate Integrin and Notch Signaling. Science 2013, 340 (6135), 991. [PubMed: 23704575]
34. Jo MH; Li J; Jaumouillé V; Hao Y; Coppola J; Yan J; Waterman CM; Springer TA; Ha TJ Single-Molecule Characterization of Subtype-Specific β1 Integrin Mechanics. Nat. Commun 2022, 13 (1), 7471. [PubMed: 36463259]

35. Dutta PK; Zhang Y; Blanchard AT; Ge C; Rushdi M; Weiss K; Zhu C; Ke Y; Salaita K Programmable Multivalent DNA-Origami Tension Probes for Reporting Cellular Traction Forces. Nano Lett 2018, 18, 4803. [PubMed: 29911385]
36. Ramey-Ward AN; Su H; Salaita K Mechanical Stimulation of Adhesion Receptors Using Light-Responsive Nanoparticle Actuators Enhances Myogenesis. ACS Appl. Mater. Interfaces 2020, 12 (32), 35903. [PubMed: 32644776]
37. Hong J; Ge C; Jothikumar P; Yuan Z; Liu B; Bai K; Li K; Rittase W; Shinzawa M; Zhang Y; Palin A; Love P; Yu X; Salaita K; Evavold BD; Singer A; Zhu C A TCR Mechanotransduction Signaling Loop Induces Negative Selection in the Thymus. Nat. Immunol 2018, 19, 1379. [PubMed: 30420628]
38. Chen Y; Li Z; Ju LA Tensile and Compressive Force Regulation on Cell Mechanosensing. Biophys. Rev 2019, 11, 311. [PubMed: 31073958]
39. Périgo EA; Hemery G; Sandre O; Ortega D; Garaio E; Plazaola F; Teran FJ Fundamentals and Advances in Magnetic Hyperthermia. Appl. Phys. Rev 2015, 2, 041302.
40. Sebesta C; Hinojosa DT; Wang B; Asfouri J; Li Z; Duret G; Jiang K; Xiao Z; Zhang L; Zhang Q; Colvin VL; Goetz SM; Peterchev AV; Dierick HA; Bao G; Robinson JT Subsecond Multichannel Magnetic Control of Select Neural Circuits in Freely Moving Flies. Nat. Mater 2022, 21, 951. [PubMed: 35761060]
41. Rosensweig RE Heating Magnetic Fuid with Alternating Magnetic Field. J. Magn. Magn. Mater 2002, 252, 370.
42. Lee JH; Jang JT; Choi JS; Moon SH; Noh SH; Kim JW; Kim JG; Kim IS; Park KI; Cheon J Exchange-Coupled Magnetic Nanoparticles for Efficient Heat Induction. Nat. Nanotechnol 2011, 6, 418. [PubMed: 21706024]
43. Jang JT; Nah H; Lee JH; Moon SH; Kim MG; Cheon J Critical Enhancements of MRI Contrast and Hyperthermic Effects by Dopant-Controlled Magnetic Nanoparticles. Angew. Chem. Int. Ed. Engl 2009, 48, 1234. [PubMed: 19137514]
44. Cardellini A; Fasano M; Bigdeli MB; Chiavazzo E; Asinari P Thermal Transport Phenomena in Nanoparticle Suspensions. J. Phys. Condens. Matter 2016, 28, 483003. [PubMed: 27701144]
45. Obaidat IM; Issa B; Haik Y Magnetic Properties of Magnetic Nanoparticles for Efficient Hyperthermia. Nanomaterials 2015, 5 (1), 63. [PubMed: 28347000]
46. Shubitidze F; Kekalo K; Stigliano R; Baker I Magnetic Nanoparticles with High Specific Absorption Rate of Electromagnetic Energy at Low Field Strength for Hyperthermia Therapy. J. Appl. Phys 2015, 117, 094302. [PubMed: 25825545]
47. Cobianchi M; Guerrini A; Avolio M; Innocenti C; Corti M; Arosio P; Orsini F; Sangregorio C; Lascialfari A Experimental Determination of the Frequency and Feld Dependence of Specific Loss Power in Magnetic Fluid Hyperthermia. J. Magn. Magn. Mater 2017, 444, 154.
48. Mohapatra J; Xing M; Liu JP Inductive Thermal Effect of Ferrite Magnetic Nanoparticles. Materials 2019, 12 (19), 3208. [PubMed: 31574950]
49. Rytov RA; Bautin VA; Usov NA Towards Optimal Thermal Distribution in Magnetic Hyperthermia. Sci. Rep 2022, 12, 3023. [PubMed: 35194138]
50. Christiansen MG; Senko AW; Chen R; Romero G; Anikeeva P Magnetically Multiplexed Heating of Single Domain Nanoparticles. Appl. Phys. Lett 2014, 104, 213103.
51. Ovejero JG; Armenia I; Serantes D; Veintemillas-Verdaguer S; Zeballos N; López-Gallego F; Grüttner C; Fuente JM; Morales MP; Grazu V Selective Magnetic Nanoheating: Combining Iron Oxide Nanoparticles for Multi-Hot-Spot Induction and Sequential Regulation. Nano Lett 2021, 21, 7213. [PubMed: 34410726]
52. Stolarczyk JK; Deak A; Brougham DF Nanoparticle Clusters: Assembly and Control Over Internal Order, Current Capabilities, and Future Potential. Adv. Mater 2016, 28, 5400. [PubMed: 27411644]
53. Singamaneni S; Bliznyuk VN; Binek C; Tsymbal EY Magnetic Nanoparticles: Recent Advances in Synthesis, Self-Assembly and Applications. J. Mater. Chem 2011, 21, 16819.
54. Polo-Corrales L; Rinaldia C Monitoring Iron Oxide Nanoparticle Surface Temperature in an Alternating Magnetic Field Using Thermoresponsive Fluorescent Polymers. J. Appl. Phys 2012, 111, 07B334.

55. Guibert C; Dupuis V; Peyre V; Fresnais J Hyperthermia of Magnetic Nanoparticles: Experimental Study of the Role of Aggregation. J. Phys. Chem. C. Nanomater. Interfaces 2015, 119 (50), 28148.
56. Serantes D; Simeonidis K; Angelakeris M; Chubykalo-Fesenko O; Marciello M; Morales MDP; Baldomir D; Martinez-Boubeta C Multiplying Magnetic Hyperthermia Response by Nanoparticle Assembling. J. Phys. Chem. C Nanomater. Interfaces 2014, 118 (11), 5927.
57. Sakellari D; Brintakis K; Kostopoulou A; Myrovali E; Simeonidis K; Lappas A; Angelakeris M Ferrimagnetic Nanocrystal Assemblies as Versatile Magnetic Particle Hyperthermia Mediators. Mater. Sci. Eng. C 2016, 58, 187.
58. Zhao J; Su H; Vansuch GE; Liu Z; Salaita K; Dyer RB Localized Nanoscale Heating Leads to Ultrafast Hydrogel Volume-Phase Transition. ACS Nano 2019, 13 (1), 515. [PubMed: 30574782]
59. Dong Y; Bazrafshan A; Pokutta A; Sulejmani F; Sun W; Combs JD; Clarke KC; Salaita K Chameleon-Inspired Strain-Accommodating Smart Skin. ACS Nano 2019, 13, 9918. [PubMed: 31507164]
60. Su H; Liu Z; Liu Y; Ma VP; Blanchard A; Zhao J; Galior K; Dyer RB; and Salaita K Light-Responsive Polymer Particles as Force Clamps for the Mechanical Unfolding of Target Molecules. Nano Lett 2018, 18, 2630. [PubMed: 29589759]
61. Huang H; Delikanli S; Zeng H; Ferkey DM; Pralle A Remote Control of Ion Channels and Neurons through Magnetic-Field Heating of Nanoparticles. Nat. Nanotechnol 2010, 5, 602. [PubMed: 20581833]
62. Nai J; Wang S; Lou XWD Ordered Colloidal Clusters Constructed by Nanocrystals with Valence for Efficient CO2 Photoreduction. Sci. Adv 2019, 5, eaax5095. [PubMed: 31853497]
63. Teich EG; Anders GV; Klotsa D; Dshemuchadse J; Glotzer SC Clusters of Polyhedra in Spherical Confinement. Proc. Natl. Acad. Sci. U. S. A 2016, 113 (6), E669. [PubMed: 26811458]
64. Ganesan V; Lahiri BB; Louis C; Philip J; Damodaran SP Size-Controlled Synthesis of Superparamagnetic Magnetite Nanoclusters for Heat Generation in an Alternating Magnetic Field. J. Mol. Liq 2019, 281, 315.
65. Wang Y; Xu F; Zhang C; Lei D; Tang Y; Xu H; Zhang Z; Lu H; Du X; Yang GY High MR Sensitive Fluorescent Magnetite Nanocluster for Stem Cell Tracking in Ischemic Mouse Brain. Nanomedicine 2011, 7, 1009. [PubMed: 21530678]
66. Isojima T; Suh SK; Vander Sande JB; Hatton TA Controlled Assembly of Nanoparticle Structures: Spherical and Toroidal Superlattices and Nanoparticle-Coated Polymeric Beads. Langmuir 2009, 25 (14), 8292. [PubMed: 19435297]
67. Fu R; Jin X; Liang J; Zheng W; Zhuang J; Yang W Preparation of Nearly Monodispersed Fe3O4/SiO2 Composite Particles from Aggregates of Fe3O4 Nanoparticles. J. Mater. Chem 2011, 21, 15352.
68. Ramey-Ward AN; Su H; Salaita K Mechanical Stimulation of Adhesion Receptors Using Light-Responsive Nanoparticle Actuators Enhances Myogenesis. ACS Appl. Mater. Interfaces 2020, 12 (32), 35903. [PubMed: 32644776]
69. Lim Y; Noh SH; Shin TH; Lee JU; Lungerich D; Lee JH; Cheon J Magnetothermally Activated Nanometer-level Modular Functional Group Grafting of Nanoparticles. Nano Lett 2021, 21, 3649. [PubMed: 33856815]
70. Azo Polymerization Initiators Comprehensive Catalog. FUJIFILM Wako Pure Chemical Corporation
71. Riedinger A; Guardia P; Curcio A; Garcia MA; Cingolani R; Manna L; Pellegrino T Subnanometer Local Temperature Probing and Remotely Controlled Drug Release Based on Azo-Functionalized Iron Oxide Nanoparticles. Nano Lett 2013, 13, 2399. [PubMed: 23659603]
72. Kopan R; Ilagan XG The Canonical Notch Signaling Pathway: Unfolding the Activation Mechanism. Cell 2009, 137 (2) 216. [PubMed: 19379690]
73. Gordon WR; Zimmerman B; He L; Miles LJ; Huang J; Tiyanont K; McArthur DG; Aster JC; Perrimon N; Loparo JJ; Blacklow SC Mechanical Allostery: Evidence for a Force Requirement in the Proteolytic Activation of Notch. Dev. Cell 2015, 33 (6), 729. [PubMed: 26051539]
74. Tagami S; Okochi M; Yanagida K; Ikuta A; Fukumori A; Matsumoto N; Ishizuka-Katsura Y; Nakayama T; Itoh N; Jiang J; Nishitomi K; Kamino K; Morihara T; Hashimoto R; Tanaka T; Kudo

T; Chiba S; Takeda M Regulation of Notch Signaling by Dynamic Changes in the Precision of S3 Cleavage of Notch-1. Mol. Cell Biol 2008, 28, 165. [PubMed: 17967888]

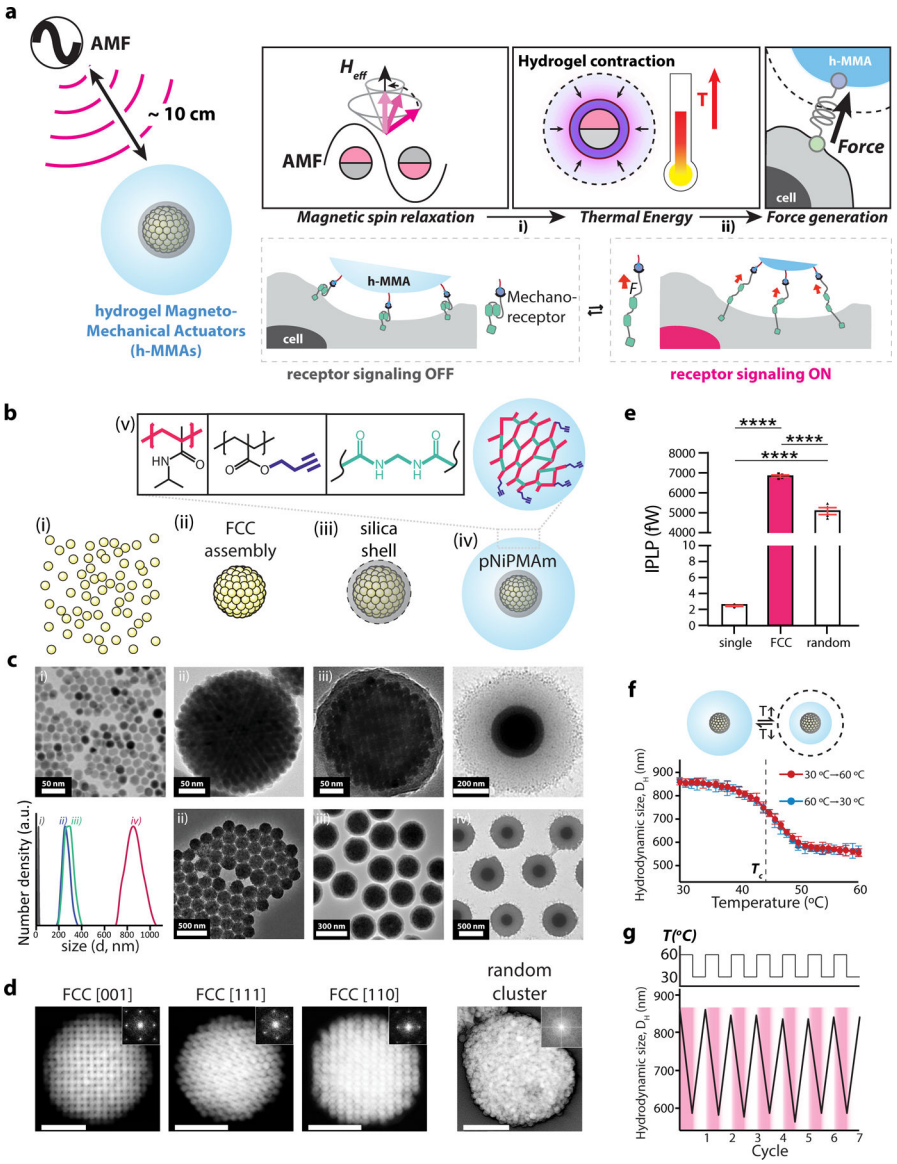

Figure 1. Design, synthesis, and characterization of hydrogel magnetomechanical actuator (h-MMA) nanoparticles.

(a) Schematic illustration showing wireless control of targeted mechanoreceptors using h-MMAs. h-MMAs exert mechanical tensile stress to target proteins in response to alternating magnetic fields via a 2-step mechanism including i) magnetic-to-thermal and ii) thermal-to-mechanical transductions. **(b, c)** Schematics and TEM images of i) 13 nm Zn-doped iron oxide ($Zn_{0.4}Fe_{2.6}O_4$) nanoparticles, ii) magnetic nanoparticle clusters (MNCs) in a face-centered cubic (FCC) superlattice structure, iii) MNC@SiO_2, and iv) MNC@SiO_2@pNiPMAm. v) Surface functionalization of h-MMAs with pNiPMAm polymer and alkyne functional group cross-linked by N, N'-methylenebisacrylamide. DLS spectra at each stage of h-MMA synthesis is also shown in the inset. **(d)** Scanning TEM images and reduced FFT images (insets) of an FCC cluster at different crystalline faces and of a random cluster. Scale bars = 100 nm. **(e)** Individual particle loss power (IPLP) values of single MNPs, FCC-structured MNCs, and random aggregates. Data are mean ± s.e.m.

from n = 4 independent trials (****p<0.0001; one-way ANOVA followed by Tukey's). **(f)** Temperature-dependent VPT of h-MMAs. The critical temperature (T_C) is marked with a black dotted line (43 ± 0.5 °C, n = 3). **(g)** Measurement of the hydrodynamic size of h-MMAs through temperature-controlled DLS measurement during 7 cycles of repeated heating and cooling.

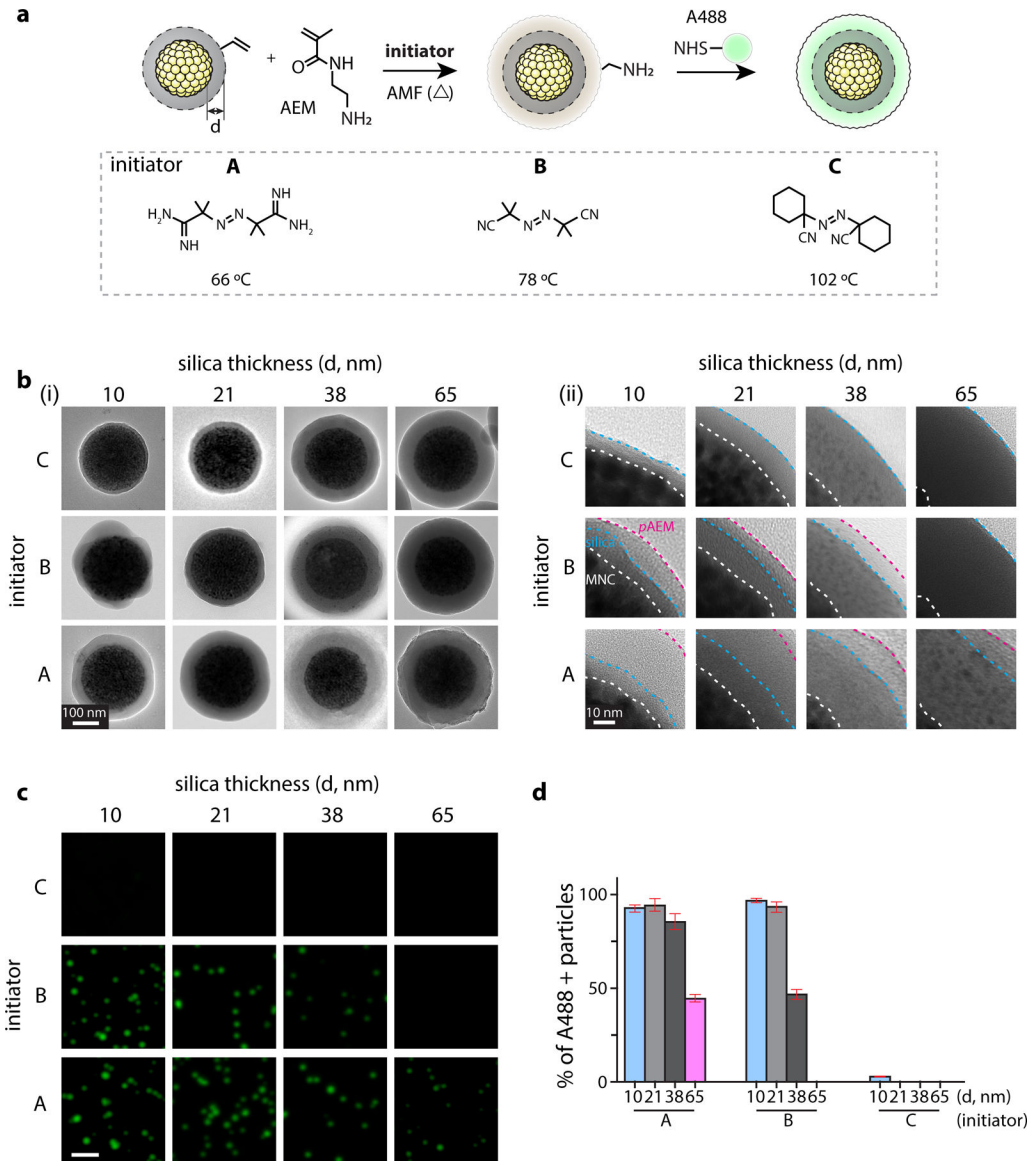

Figure 2. Thermal polymerization of N-(2-aminoethyl)methacrylate (AEM) on MNC@SiO_2 to investigate AMF-induced local heating effects by MNCs.

(a) (top) Schematic illustrations of radical polymerization of AEM and subsequent conjugation of amine-reactive fluorescence dyes within it. We varied the SiO_2 layer thickness (d = 10, 21, 38, 65 nm) to investigate distance-dependent thermal decay from MNC surface. **(bottom)** Three thermo-labile azo-molecule initiators with varied decomposition temperatures for AEM polymerization: A, 2,2′-azobis(2-methylpropionamidine) dihydrochloride; B, 2,2′-azobis(2-methylpropionitrile); C, 1,1′-azobis(cyclohexanecarbonitrile). **(b)** Representative TEM images (Left: entire particle view, Right: zoom-in view) after AMF-stimulation in presence of respective MNC@SiO_2 particles and initiators. Scale bar = 100 nm. Interface of MNC/SiO_2, SiO_2/*p*AEM, and AEM/vacuum (white dotted line) are marked by white, blue, magenta dotted lines, respectively. Scale bar = 10 nm. **(c)** Fluorescence signals of the Alexa488-positive particles prepared with radical polymerization conditions shown in Figure 2b and subsequent conjugation of A488–NHS.

The images were acquired with a 488-nm laser and FITC emission filter. Scale bar = 2 μm. **(d)** Fraction analysis of A488-positive particles. Fluorescence-positive particles were identified by using a threshold calculated as mean ± 3×SD of basal signal intensity. Data are mean ± SD from n = 3 independent experiments.

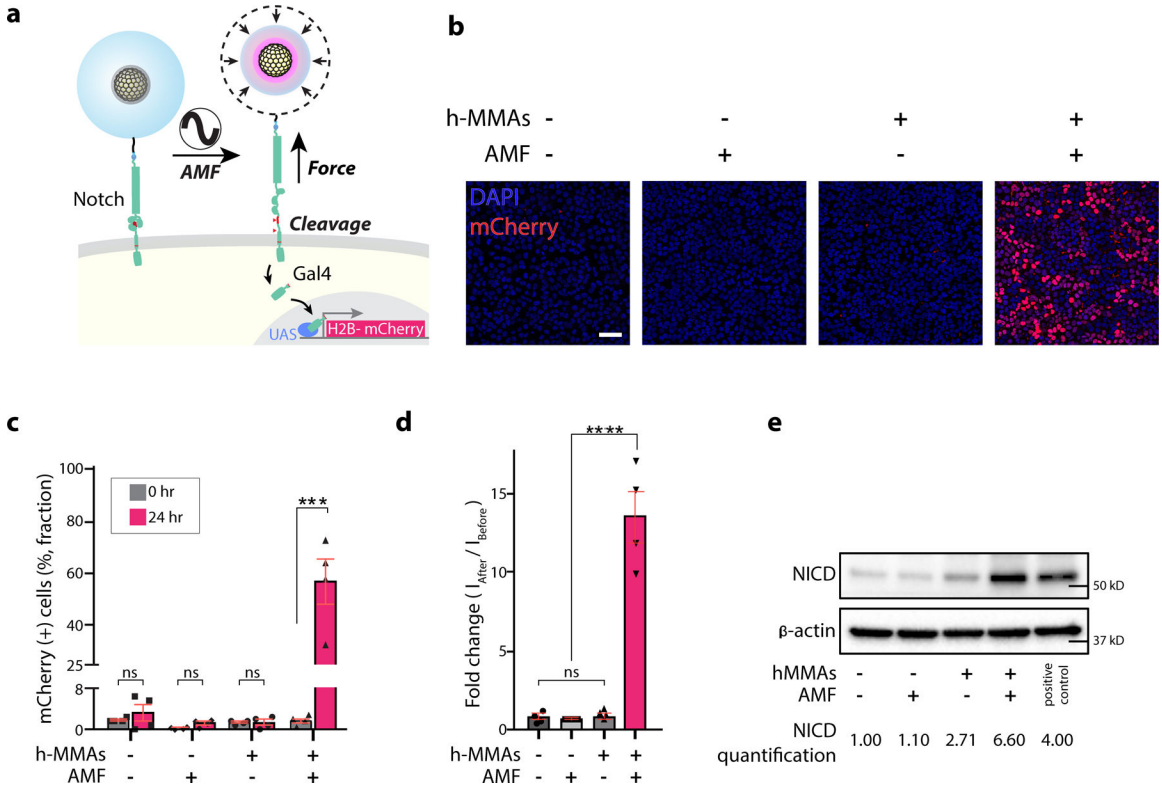

Figure 3. AMF-induced activation of Notch signaling in a cell line model using h-MMA nanoparticles.

(a) A schematic illustration of h-MMAs induced activation of U2OS reporter cells expressing SNAP-Notch1-Gal4 and H2B-mCherry. h-MMAs specifically label Notch1 receptors via SNAP-benzylguanine (BG) chemistry. AMF stimulation (50 kHz at 500 Oe, 30 s ON / 2 min OFF cycle for 15 times) induced VPT and exerted mechanical force to Notch1. Mechanical stimulation of Notch1 triggers enzymatic cleavages of Notch1 and downstream transcription of H2B-mCherry. **(b)** Representative confocal fluorescence images of the reporter cells treated with h-MMA nanoparticles and AMF. Cells treated with no h-MMA or AMF were used as controls. Scale bar = 100 μm. **(c)** Percentage of the mCherry-positive cells with or without AMF stimulation or h-MMA treatment. Fluorescence-positive fractions were measured at (0 hr) and 24-hr post stimulation. Data are mean ± SD from n = 4 biological replicates (ns, non-significant; ***$p < 0.001$; two-tailed Student's t-test). **(d)** Normalized fold-change in mCherry fluorescence signal observed at 24-hr post-AMF stimulation as compared to the baseline level for respective experimental conditions. Data are mean ± SD from n = 4 biological replicates (ns, non-significant; ****$p < 0.0001$; two-tailed Student's t-test). **(e)** Immunoblot analysis of cleaved Notch intracellular domain (NICD). β-actin levels represent the loading control. The number below the gel images indicates the relative NICD band intensity. The intensity of each NICD band relative to the respective β-actin band was quantified and normalized to that of the control groups treated with no h-MMAs or AMF.

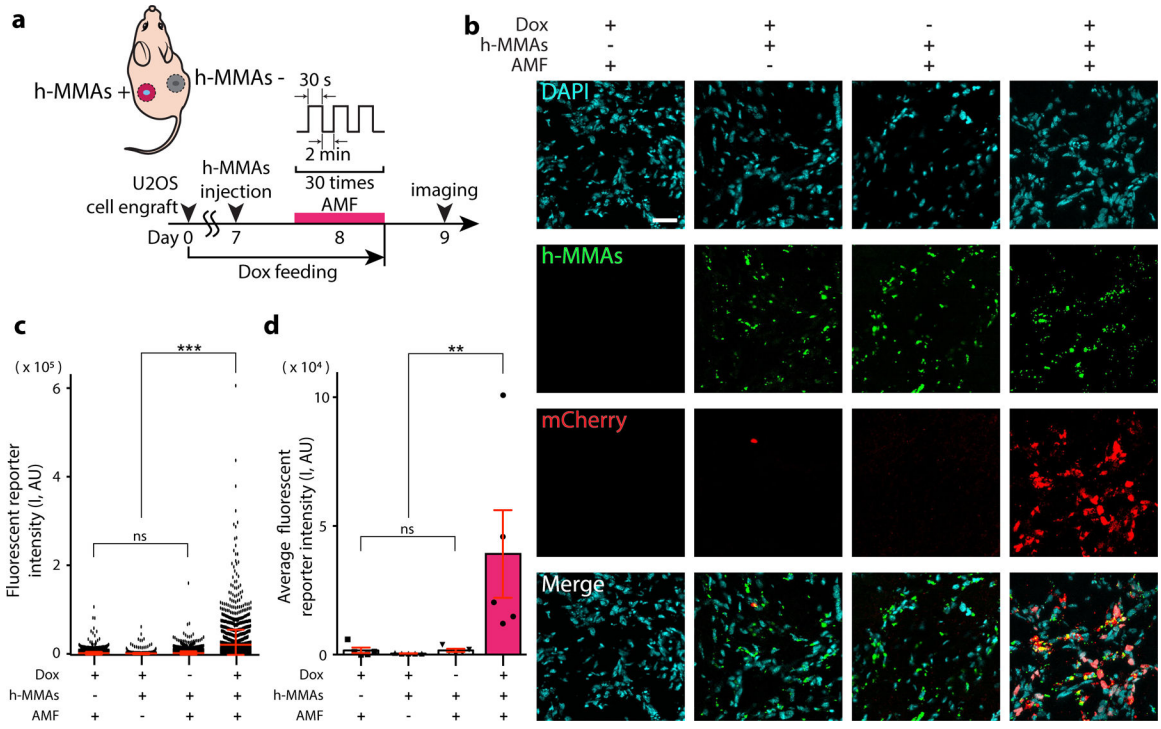

Figure 4. Minimally invasive remote control of cells expressing Notch receptors using h-MMA nanoparticles.

(a) A schematic illustration of AMF-induced h-MMA stimulation using a xenograft mouse model. Fluorescent reporter Notch1-U2OS cells were implanted on both sides of the mice on day 0. Mice were provided with a doxycycline (Dox, 2 mg/ml) diet for Notch receptor expression. One week later, h-MMAs were directly injected into the center of the xenograft, and AMF was applied to the xenograft position. On Day 9, mice were sacrificed and cryosectioned tissues were prepared for immunohistochemical analyses. **(b)** Representative confocal fluorescence images of tumor sections with AMF and h-MMA treatment. Substantial mCherry (red) expression was observed only in the presence of h-MMAs (green), Dox treatment, and AMF. DAPI (blue), Scale bar = 40 μm. Tumors with no AMF or h-MMA treatments were used as negative controls. **(c)** Quantification of nuclear mCherry signal per single cell in the representative slices where h-MMAs were localized. Data are mean ± s.e.m. from n = 2,300 cells from 5 animals (ns, non-significant; ***p<0.005; one-way ANOVA followed by Tukey's). **(d)** Quantification of average nuclear mCherry fluorescence intensity. Data are mean ± SD from n = 5 animals (ns, non-significant; **p<0.005; one-way ANOVA followed by Tukey's).